



Effects of rapid calcination on properties of calcium-based sorbents

Chang-Feng Yan^{a,b,*}, John R. Grace^a, C. Jim Lim^a

^a Department of Chemical & Biological Engineering, University of British Columbia, Vancouver, Canada V6T 1Z3

^b Guangzhou Institute of Energy Conversion, Chinese Academy of Sciences, Guangzhou 510640, China

ARTICLE INFO

Article history:

Received 15 May 2010

Received in revised form 24 June 2010

Accepted 2 July 2010

Keywords:

Rapid calcination

Calcium-based sorbents

Foil

Wire mesh

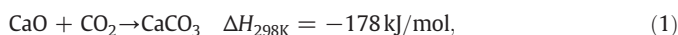
ABSTRACT

The calcination process may influence subsequent fragmentation, sintering and swelling when CaO derived from limestone acts as a CO₂ or SO₂-sorbent in combustion, gasification and reforming. Sorbent properties are affected by CO₂ partial pressure, total pressure, temperature, heating rate, impurities and sample size. In this study, the effect of calcination heating rate was investigated based on an electrically heated platinum foil. The effects of heating rate (up to 800 °C/s), calcination temperature (700–950 °C), particle size (90–180 μm) and sweep gas velocity were investigated. Higher initial heating rates led to lower extents of limestone calcination, but the extents of carbonation of the resulting CaO were similar to each other. Calcium utilization declined markedly during carbonation or sulphation of CaO after calcination by rapid heating. Experimental results show that carbonation and calcium utilization were most effective for carbonation temperatures between 503 and 607 °C. Increasing the extent of calcination is not the best way to improve overall calcium utilization due to the vast increase in energy consumption.

© 2010 Elsevier B.V. All rights reserved.

1. Introduction

The increasing use of fossil fuels to meet energy needs has led to higher carbon dioxide (CO₂) and sulphur dioxide (SO₂) emissions into the atmosphere. Increasing attention has been focused on chemical looping of limestone involving calcination and carbonation for carbon dioxide separation during combustion, gasification and reforming. Gaseous CO₂ reacts with lime to yield calcium carbonate during carbonation



and the lime is then regenerated by calcination, i.e.



Lime derived from calcium-based sorbent (limestone or dolomite) is also commonly utilized to capture SO₂ in fluidized bed combustors via



It is important to understand whether the manner in which the calcination takes place affects the subsequent carbonation and sulphation processes. In this paper, we investigate the effects of

calcination rate and conditions on the subsequent performance of calcium-based sorbents.

2. Calcination

Calcination of limestone involves five steps:

- (1) Heat transfer from the surroundings to the exterior of a particle.
- (2) Heat transfer from the external surface to the interior reaction interface.
- (3) Heat absorption and thermal decomposition at the reaction interface.
- (4) Diffusion of CO₂ formed by the reaction through a porous layer of CaO.
- (5) Diffusion of CO₂ from the particle exterior surface to the surroundings.

Several investigations [1,2] have shown that decomposition of calcium carbonate occurs at a well-defined boundary between the CaO and CaCO₃ phases. This boundary migrates towards the centre of the particle. Dennis and Hayhurst [3] and Silcox et al. [4] used the shrinking core model to predict their experimental results, whereas Borgwardt [5] assumed a homogeneous reaction throughout the sorbent for particles smaller than 90 μm. Khinast et al. [6] concluded that simple models such as the shrinking core and uniform conversion models only apply in extreme cases. Rao et al. [7] assumed gradual conversion in pellets of size ~6.5 mm, with the mass transfer in the porous shell controlling the reaction. Later, Hu and Scaroni [8]

* Corresponding author. Guangzhou Institute of Energy Conversion, Chinese Academy of Sciences, Guangzhou 510640, China. Tel./fax: +86 20 8705 7729.

E-mail address: yancf@ms.giec.ac.cn (C.-F. Yan).

observed by SEM analysis different conversion levels inside partially calcined 63 μm limestone particles.

Both heat and mass transfer have been found to influence the rate of calcination. Improved thermal conductivity of the selected sweep gas increases the rate of calcination [9]. Previous studies [2,10,11] have indicated that the kinetics of decomposition of calcium-based sorbents depend greatly on the experimental system and conditions.

The porosities of calcined samples vary over a wide range (0.32–0.51) depending on the limestone. The apparent activation energies of large limestone particles calcined in thermogravimetric analyzers or in differential reactors at temperatures <900 °C range from 79 to 280 kJ/mol [5,7,11–15], while the activation energy has been determined to be 209 kJ/mol [16,17]. Garca-Calvo et al. [15] found values from 110 to 194 kJ/mol depending on the limestone impurities. These values are higher than those (33 to 92 kJ/mol) obtained in entrained-flow reactors [4,14,18] for particles smaller than 100 μm and temperatures up to 1200 °C. Mai [19] attributed the higher activation energies to inadequate sorbent/gas mixing or slow particle heat-up. Results were similar for dehydration of calcium hydroxide. Activation energies between 79 kJ/mol [12] and 280 kJ/mol [13] were higher than ~67 kJ/mol obtained in a drop tube reactor [14,19]. The activation energy for calcination of Omyacarb limestone, 96 kJ/mol, was similar to that obtained by other authors under similar experimental conditions. However, values of 36 and 50 kJ/mol, reported by Fierro et al. [20], were lower than those obtained by other authors.

Khraisha and Dugwell [21] studied the thermal decomposition of a limestone in a thermogravimetric analyzer at heating rates up to 80 K/min and temperatures to 950 °C. They also summarized a wide range of data from other workers with activation energies and frequency factors varying from 33 to 4002 kJ/mol and 10^2 to 10^{69} s^{-1} , respectively.

Particle size influences the calcination rate. For small particles (1–90 μm), chemical reaction controls the calcination rate [5,14]. Heat transfer becomes important [7] for particles larger than 6 mm. For intermediate size particles, reaction and internal mass transfer are the main resistances controlling calcination. Their relative importance also depends on the pore structure. The calcination rate increases with decreasing particle size because pore diffusion is less important for smaller particles. The relative importance of heat transfer is also greatly influenced by particle size [6,8,22].

From the numerical simulation of Hu and Scaroni [8], the intraparticle average temperature is lower than the sweep gas temperature, and there are large temperature gradients within the particle, especially for larger particles. Wernick [23] attributed the difference between activation energies of limestones to different calcination temperatures. He proposed that the activation energy is higher at low temperatures. Bischoff [24] found an activation energy of 185 kJ/mol in the temperature range between 550 and 800 °C in moist or dry sweep air, whereas Ar and Dogu [25] obtained values between 410 and 1470 kJ/mol, depending on the heating rate and gas composition.

3. Carbonation

The possibility of using the carbonation reaction to capture CO_2 from a gas stream was considered as early as the 19th century [26]. Calcined limestone may be able to remove CO_2 in fluidized bed combustion environments and, by subsequent calcination, to produce a nearly pure CO_2 stream for sequestration in a chemical looping process [27–30]. This scheme involved a fluidized bed combustor-carbonator where the fuel burned in an excess of lime which, depending on operating conditions, removed 80% or more of the CO_2 and effectively all of the SO_2 , and a calciner where sorbent was regenerated releasing a gas of high CO_2 concentration. However,

experimental results indicate a rapid decline in sorbent effectiveness, especially if SO_2 is present [31].

Carbonation involves three different processes according to the unreacted shrinking core model, any of which can be rate-controlling:

- (1) Mass transfer from the gas phase to the surface.
- (2) Diffusion of gaseous reactant inside the particle pores or through the product layer.
- (3) Chemical reaction.

The gas–solid CO_2 –CaO reaction proceeds through two rate-controlling regimes [32,33]. Reaction occurs rapidly by heterogeneous reaction at the surface in the initial stage. A compact layer of product CaCO_3 then develops on the outer region of the particle, causing the rate of reaction to decrease due to the diffusion limitation through this layer [33]. The reaction does not proceed to complete conversion of CaO, instead giving ultimate conversions of 70–80% [34] or up to 90% [35]. To describe such gas–solid reaction kinetics, various models have been proposed.

Structural limitations prevent the attainment of 100% conversion. Dedman and Owen [36] obtained a CO_2 uptake of about 0.23 g of CO_2 /g of CaO (~30% conversion) in 30 min at 600 °C. Bhatia and Perlmutter [34] reached ~70% conversion for 81–137 μm particles. Mess et al. [37] reported 82% conversion at 1050 °C and 11.74 atm CO_2 pressure after 32 h for 15–20 μm particles. The limitation on total conversion stems essentially from the initial pore size distribution of the CaO sorbent. Microporous sorbents (pore size <2 nm) are very susceptible to pore blockage and plugging through formation of a higher-molar-volume product (molar volume of CaO = 17 cm^3/mol , whereas molar volume of CaCO_3 = 37 cm^3/mol). CaO sorbents from naturally-occurring precursors are usually microporous. At the end of the kinetically controlled regime, diffusion through the product layer controls the reaction rate. Wei et al. [38] suggested that a mesoporous structure which maximizes porosity in the 5–20 nm pore size range would be less susceptible to pore plugging, while providing sufficient surface area to ensure rapid kinetics. The modified precipitation technique [32] resulted in a mesoporous CaCO_3 structure with high BET surface area (60 m^2/g). Barker [39] obtained repeated 93% conversions over 30 cycles at 629 °C on 10 nm CaO particles. Gupta and Fan [35] modified calcium carbonate precipitation to achieve higher (>90%) carbonation conversions.

4. Reactors for calcination

To develop accurate predictive models and to simulate the calcination process, it is necessary to measure the reaction rate as a function of time and temperature. Heating rates can vary from fractions to tens of thousands of °C/s. The reaction is affected by a combination of heat transfer, mass transfer and chemical reaction, which are in turn affected to different extents by such factors as particle physical shape, heat capacity, emissivity and thermal conductivity.

A variety of reactors have been employed including induction heating, laser heating, fluidized beds, plasma and shock tubes, entrained-flow reactors, and wire-mesh reactors. An electrically heated wire-mesh reactor was first used by Loison and Chauvin [40]. They were subsequently widely employed in coal kinetics studies, e.g. by Anthony et al. [41,42], Suuberg [43] and Fong [44] at MIT; Gibbins et al. [45–47], Kandiyoti [48,49] at Imperial College, and Mill [50] at the University of New South Wales. The time of heating in this type of apparatus can be precisely controlled, and good material balances can be obtained, to an accuracy of a few percent [51]. The fundamental problems are the weighing and measurement of particle temperature during heat-up and calcination. The thermal properties and thermal response of the particles may differ significantly from the thermocouple attached to the wire mesh. These differences are important if a significant temperature gradient exists between the

screen and the sample, in which case particle temperature is not known accurately during heating. Welding of a thermocouple to the mesh can also affect the local properties of the mesh, resulting in hot or cold spots. The diameter of the thermocouple wire and bead diameter should be comparable to the sorbent particle diameter, or smaller to reduce the ratio of the heat capacity of a thermocouple bead to that of the sorbent particle. When the sorbent particle emissivity exceeds that of the thermocouple, the sorbent may track the mesh temperature better than the thermocouple at high temperature, as radiation becomes more important than gas phase conduction [51]. It is also important, but difficult in practice, to form a thin mono-layer of sorbent on the mesh to avoid piling (i.e. more than one particle deep), which would increase the difference between the measured and actual particle temperatures.

Mill [50] reported a 0.2 s lag, corresponding to a 200 °C temperature gap, between the heating wire mesh and coal particle temperature for heating rates up to 1000 °C/s. This difference was partly due to the difference between the signal responses of two thermocouples. The response time of the thermocouple was slower than that of the mesh due to different thermal conductivities and heat capacities. The temperature history of the coal experienced a lag, with the shape of the curve remaining similar to that of the mesh at temperatures >400 °C. A period of time with the mesh held at constant temperature is needed for the particle to reach the desired maximum temperature.

5. Experimental system

Fig. 1 shows the electrical circuit. A stainless steel wire mesh was used initially, but the stainless steel was then replaced by a platinum foil to avoid oxidation at high temperatures, which could affect the weight measurements.

Stainless steel screen of 325 mesh with nominal 44 μm openings and 30 μm wire diameter was cut into 50×50 mm squares and symmetrically folded, whereas platinum foil of thickness 0.025 μm was cut into 25×50 mm pieces. Sorbents were spread on a 20×20 mm rectangular section in the centre of the folded mesh or at the centre of platinum foil. The mesh or foil was held between brass clamps, and heated by direct current. A 165 μm diameter type-R thermocouple bead was welded to the mesh or the foil to measure and

control the mesh temperature. Industrial nitrogen sweep gas (99%) flowed through the mesh or over the foil to remove product gas from the surface of the particles.

The DC power supply was a 12-volt automobile battery. Control of the final temperature of the mesh or foil was preset at the specified current through the mesh or foil by 5 rheostats in parallel, each with a maximum rating of 300 W (1 Ω). At atmospheric pressure, a final temperature of 800–900 °C was maintained for 10–80 s after heating at nominal heating rates of 0.1 to 1000 °C/s. The heating circuit consisted of two branches, one controlling the heating rate, whereas the second maintained the final temperature at 800–900 °C. A superficial sweep gas velocity of 0.1 m/s was used as in previous work [45–47], which showed that this is the lowest velocity to give reliable product removal at higher heating rates. Properties of the foils were relatively invariant during heating to 1500 °C. To prevent sagging and buckling of the mesh, one electrode was spring-loaded so that the mesh was taut throughout the run, as in a previous study [44].

The resistivity of stainless steel is nearly 6 times that of platinum at room temperature. The available heating rate sharply decreases as the sample temperature increases. In the experiments of Anthony et al. [41] and Suuberg et al. [43], the heating rate was up to 10,000 °C/s for <0.1 s, with ~10–15 mg of powdered coal spread in a layer one or two particles deep on a pre-weighed screen. Limestone calcination occurs mainly between 700 and 900 °C. Higher temperatures make uniform heating more difficult because radiation heat losses depend on the fourth power of the absolute particle temperature. Resistivity of the material also increases with increasing temperature, necessitating a wide range of power and voltage.

Sorbents were tested in the UBC dual-environment thermogravimetric reactor (TGR) described by Laursen et al [52]. Sample particles (0 to 180 μm) were spread evenly in a stainless steel basket suspended in a vertical cylindrical electrical furnace of 50 mm inside diameter. The simulated flue gas was drawn from four cylinders containing different combinations of CO₂, air, N₂ and SO₂. Mass flow meters measured and controlled the individual gas flows. A removable top section, including the sample holder, and a removable bottom section holding a thermocouple tube were attached to the main body of the reactor by ground joints. Samples could be unloaded and re-loaded by removing the top section. Introduced through the inlet at the bottom of the reactor, premixed gas contacted the sample

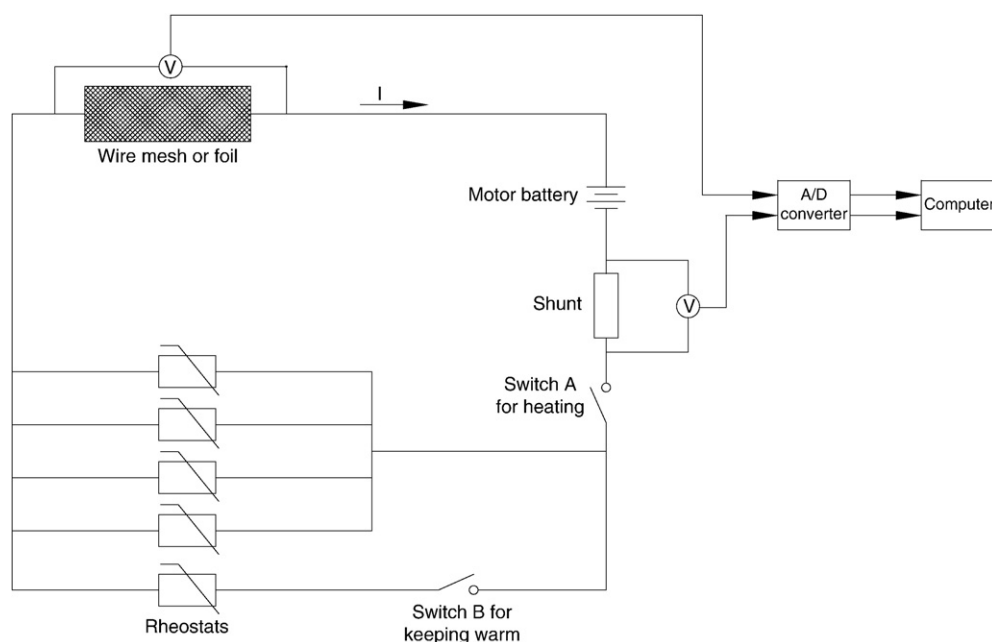


Fig. 1. Experimental heating circuit.

particles. K-type thermocouples, inserted from the bottom, measured the temperature of the incoming gas. A pressure transducer recorded the pressure of the inlet gas upstream. Before each test, the gas stream by-passed the reactor for several minutes to adjust the inlet CO₂ concentration. Calcium utilization was determined by logging sample weights using a load cell with an accuracy of ±0.1 mg.

It is difficult to know the emissivity of the sample accurately for non-contact surface measurements. This may cause greater error than the difference between the temperatures of the wire mesh and the sample. The coal particle temperature can be estimated by comparing the amplitude of the radiance per unit surface area and a black-body at a single frequency or at different frequencies [51]. Pyrometry methods generally assume emissivity and radiance of the particle surface. The temperature measurement is believed to be accurate to ±50 °C over the temperature range 950–1650 °C. Below 950 °C the signal was too weak for accurate measurements, so the particle temperature had to be estimated from the energy conservation equation [53]. Type R (Platinum vs. Platinum/Rhodium 13%) thermocouples are suitable for high temperatures, with a maximum temperature >1600 °C. However, their output vs. temperature is very non-linear requiring special calibration.

A 165 μm-diameter wire of 100% platinum and a 165 μm-diameter wire of 87% platinum and 13% rhodium were melted into a bead of 650 μm diameter, which was then welded to the top of the mesh or foil. Effective single-point welding made it possible to avoid interference from voltage gradients through the mesh or foil.

The electrical current through the wire-mesh circuit exceeded 50 A. Approximately 10–200 mg of ground sorbent were carefully spread across the interior of a pre-weighed mesh or foil, which was then folded twice to form a 20 × 50 mm strip. The thickness of the sample layer was 25–500 μm, a compromise between efficiency of heat and mass transfer on the one hand, and weighing accuracy on the other. A crucible to hold the sample, the sample itself, the empty mesh or foil, and a glass vessel were separately weighed on an analytical balance to ±0.1 mg. The Pt-Pt/Rh13% thermocouple was then affixed to the top of the mesh or foil. After heating, the sample remaining on the mesh and mesh were put into a glass vessel and re-weighed to determine the weight loss due to calcination. The product was then transferred to sample bottles in a sealed nitrogen plastic bag and stored in a desiccator. The limestone composition is provided in Table 1.

6. Results and discussion

Limestone was rapidly heated by the electrically heating wire-mesh reactor (WMR) and platinum foil reactor (PFR) to determine the effects of decomposition rate on the properties of calcium-based sorbents. The effects of heating rate (0–800 °C/s), final calcination temperature (700–950 °C), particle size (90–180 μm) and velocity of nitrogen sweep gas (0.1–0.51 m/s) were investigated.

Effective power and power loss are given by

$$P_{\text{mesh}} = I \cdot V_{\text{mesh}} \quad (4)$$

$$P_{\text{loss}} = I \cdot (V_{\text{total}} - V_{\text{mesh}}) \quad (5)$$

where $I = V_{\text{shunt}}/R_{\text{shunt}}$ and $R_{\text{mesh}} = V_{\text{mesh}}/I$. R_{shunt} the standard shunt resistance value at room temperature was re-calibrated before each

Table 1
Metal content of Thames limestone.

	Ca	Mg	Al	Fe	Na	K	Ti
%	38.87	0.44	0.21	0.09	0.07	0.12	0.01
		V	Sr		Ba		Ni
mg/kg		<10	179		69		<20

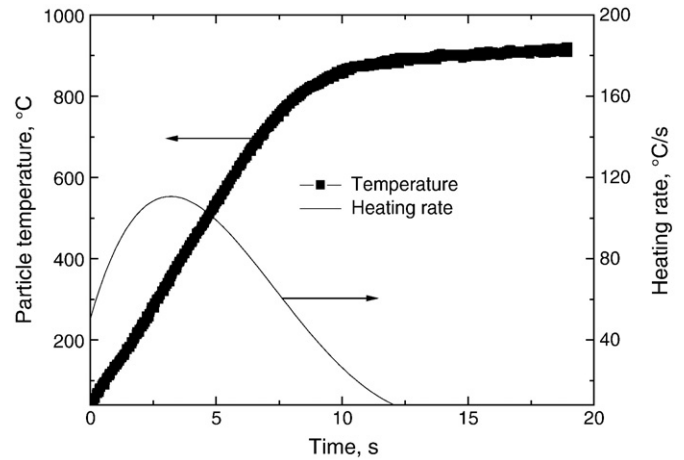


Fig. 2. Typical temperature–time trajectory during heating of 200 mg of 63–75 μm CaCO₃ particles on a wire mesh.

test. V_{total} is the total voltage provided by the motor battery, V_{mesh} the voltage across the mesh or foil, and V_{shunt} the voltage across the shunt. All voltages were recorded by the computer. P_{mesh} is the effective instantaneous power dissipation for the mesh or foil, P_{loss} the power loss for the heating circuit, and I the current through the circuit.

Typical temperatures and heating rates are shown in Fig. 2. In this case, the wire mesh holding 200 mg of 63–75 μm diameter CaCO₃ particles was heated to 900 °C at a maximum heating rate of 110 °C/s. The wire mesh was then maintained at 900 °C for 10 s. During repeated heating, the weight loss of the samples was determined after different times at the same operating conditions, as shown in Fig. 3. Weight loss became rapid when the temperature reached 900 °C. The calcination extent was defined and fitted by

$$\text{Calcination extent} = \frac{\text{Limestone calcined}}{\text{Initial limestone}} = 4.9 \ln(t/0.5). \quad (6)$$

The original sample mass was ~10 times that in the MIT tests. The heating power and heat loss are affected significantly by radiation heat losses and by heat absorption due to the endothermic calcination reaction. The heating rate was smaller for larger samples.

Nitrogen at 1000 ml/min with 0.51 m/s velocity swept the product CO₂ during the calcination in the TGR. CO₂ was added to the nitrogen flow during the carbonation stage, after opening a solenoid valve; the corresponding superficial sweep gas velocity was 0.60 m/s with the CO₂ concentration maintained at 14.4% in the

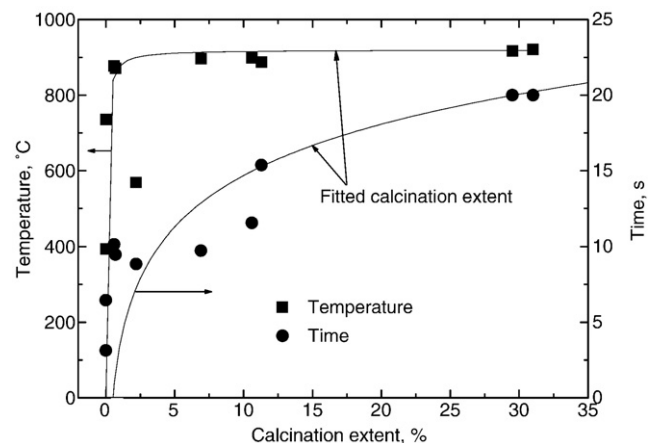


Fig. 3. Weight loss and calcination extent vs. time for maximum heating rate of 110 °C/s on a wire mesh.

incoming gas. The initial heating rate was up to 700 °C/s, followed by slower heating, due to higher radiation heat losses at higher temperature. When the temperature reached 850 °C, the temperature was then maintained at 850 °C for 70 s. A typical temperature–time trace for calcination and subsequent carbonation is plotted in Fig. 4.

From the experimental results, the highest calcium utilization was achieved for a carbonation temperature of ~607 °C, as shown in Fig. 5, where

$$\text{Overall Ca utilization} = \frac{\text{Ca present as calcium carbonate after calcination and carbonation}}{\text{Ca in original limestone}} \quad (7)$$

Except in one case specified below, all results in this paper are for the first stage of calcination/carbonation, i.e. there was no previous carbonation before calcining or carbonating the samples. Calcium utilization during carbonation and overall Ca utilization of the limestone achieved their highest levels for a carbonation temperature range of 503 to 607 °C.

The initial carbonation rate decreased significantly and the reaction was very low when the carbonation temperature was 410 °C. At a carbonation temperature of 708 °C, the carbonation rate again significantly decreased, but reaction proceeded slowly, with the overall Ca utilization reaching 80% after 45 min, nearing the level reached within 8 min for carbonation at 600 °C. Carbonation was faster at the beginning, with its rate rapidly dropping from ~0.60 mol/(mol s) to ~0.04 mol/(mol s) within 300 s for carbonation temperatures of 503 to 607 °C. The carbonation proceeded at a nearly constant low rate of 0.045 mol/(mol s) for a carbonation temperature of 708 °C, as shown in Fig. 6.

Limestone calcination rates for different-diameter particles are shown in Fig. 7 for a maximum heating rate of 10 °C/s. The calcination rates for the 106–125 µm and 125–150 µm fractions were higher than for the smaller and larger size ranges, presumably due to complex non-linear interactions among heat transfer, mass transfer and such particle properties as internal porosity and pore size [54,55].

Fig. 8 shows that limestone calcined at up to 10 °C/s could not maintain high carbonation rates. Calcination began to occur from the outer surface of particles, leading to higher CaO concentrations in their outer layers. Subsequent carbonation of CaO began at the outside, so carbonation rates fell with time as gaseous diffusion through the outer carbonate layer became rate-limiting.

Fig. 9 shows that the (stagewise) Ca utilization of CaO, defined as

$$\text{Ca utilization of CaO} = \frac{\text{Ca carbonated during carbonation}}{\text{Ca present as CaO before that carbonation}} \quad (8)$$

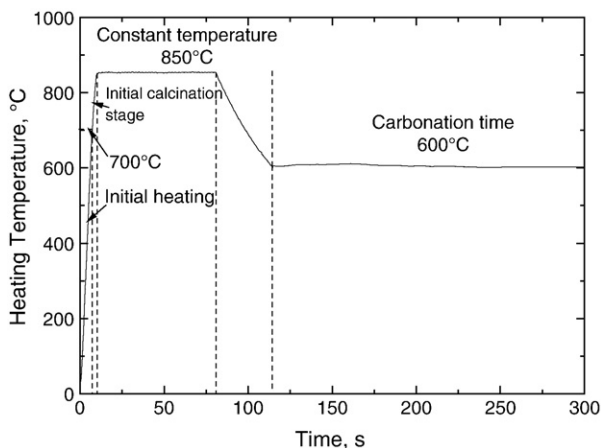


Fig. 4. Temperature–time traces during limestone calcination followed by cooling to 600 °C and carbonation.

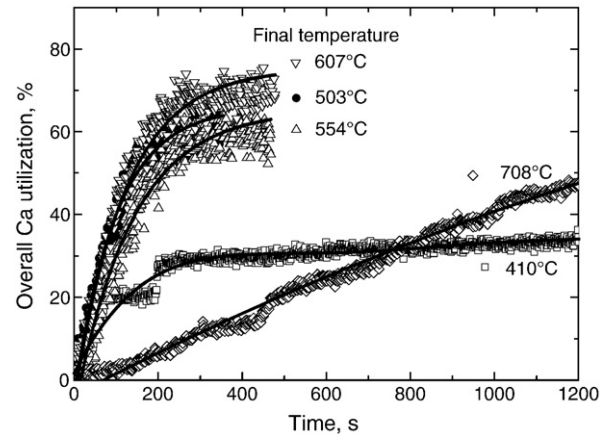


Fig. 5. Overall Ca utilization for different carbonation temperatures after maximum heating rate during calcination of 10 °C/s; particle diameter 75–90 µm; superficial sweep gas velocity 0.51 and 0.60 m/s for calcination and carbonation, respectively.

was similar to the overall Ca utilization of limestone, defined by Eq. (7) for the different particle sizes tested, both being significantly less than the calcination extent defined by Eq. (6).

The micropore structure of CaO formed during calcination is very susceptible to blockage or plugging by higher-molar-volume calcium carbonate produced from carbonation as the CaCO₃ product layer thickness increases. Accordingly, the carbonation rate experiences rapid attenuation.

When limestone particles smaller than 63 µm were calcined at a maximum heating rate of 10 °C/s for a duration sufficient to give calcination extent of 62–66%, the overall Ca utilization of limestone in the subsequent carbonation was ~48%, as shown in Fig. 10. The overall Ca utilization of limestone after 21.3% extent of calcination was only ~15%. However, the corresponding Ca utilizations of CaO (Eq. (8)) after different extents of calcination were nearly identical and up to ~70%.

When 63–75 µm limestone particles were 100% calcined at a maximum heating rate of 10 °C/s, the overall Ca utilization of the limestone increased, as shown in Fig. 11, but the Ca utilization of CaO was relatively low. The heat required for calcination tripled when the extent of calcination increased from 32.5% to 100%, but the Ca utilization of the limestone only doubled. This indicates that increasing the calcination extent may not be the best way of improving Ca utilization.

Bortz and Flament [56] reported 70% calcination of Ca(OH)₂ particles within the first 25 ms at 600 °C. Mai and Edgar [11] reported

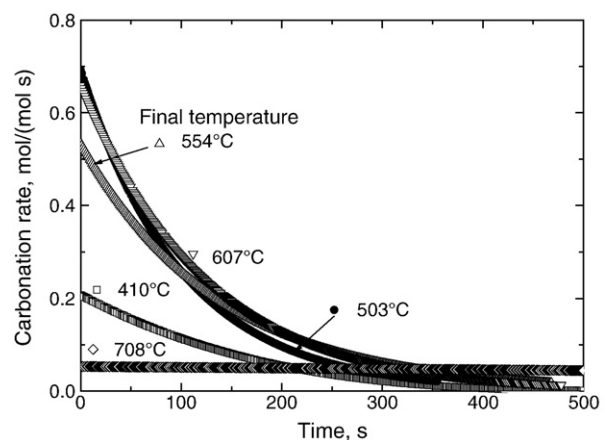


Fig. 6. Carbonation rates for different carbonation temperatures after calcination at maximum heating rate 10 °C/s; particle diameter 75–90 µm; superficial sweep gas velocity 0.51 and 0.60 m/s for calcination and carbonation, respectively.

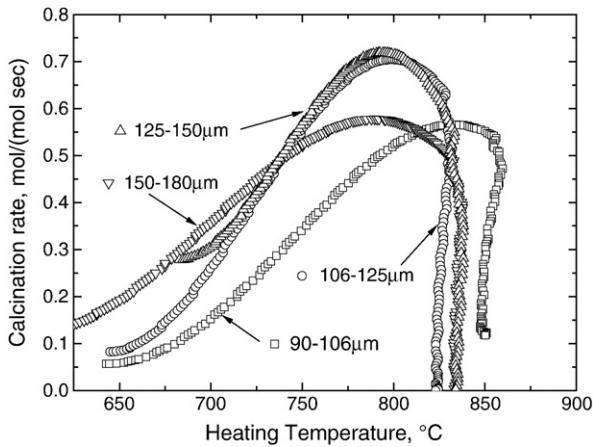


Fig. 7. Calcination rates vs. heating temperature for particles of different size ranges. Heating rate 10 °C/s; final temperature 850 °C; superficial sweep gas velocity 0.51 and 0.60 m/s for calcination and carbonation, respectively.

a slower decomposition rate, 35% calcination within 100 ms at 1152 °C for reagent-grade hydroxide powder (mass median diameter = 12.5 μm). Studies showing thermal sintering for such brief times are scarce. Very fast sintering leads to rapid reduction in surface area within 100–200 ms. Initial rapid heating adversely affects the calcination rate and extent of carbonate formation.

Limestone particles of diameter <63 μm were calcined at different heating rates to nearly the same degree of calcination. The limestone was then heated to 850 °C in the PFR at a maximum heating rate of 300 °C/s and then held at 850 °C for 70 s. The overall maximum Ca utilization of the limestone for carbonation at 600 °C was then 29%, as shown in Fig. 12. However, the Ca utilization reached 43% when the maximum heating rate during calcination was 2.25 °C/s, again indicating that the Ca utilization significantly increased when the calcination heating rate decreased.

When limestone particles of diameter 63–75 μm were heated to 850 °C in the PFR at up to 750 °C/s (see Fig. 13) and then held at that temperature for 70 s, the extent of calcination was 29.3%, and the corresponding overall Ca utilization for carbonation was then only 9.5%, as shown in Fig. 14. These data are much less than the calcination extent of 33.5% and overall Ca utilization of 22.1% in Fig. 14 for a greatly reduced heating rate in the TGA (plotted in Fig. 13). The corresponding (stagewise) Ca utilization of CaO was 33.8% for rapid heating, compared with 63.8% for the much lower-heating rate.

Fig. 15(b) presents results showing the effect of the initial calcination stage of <63 μm particles for two different heating

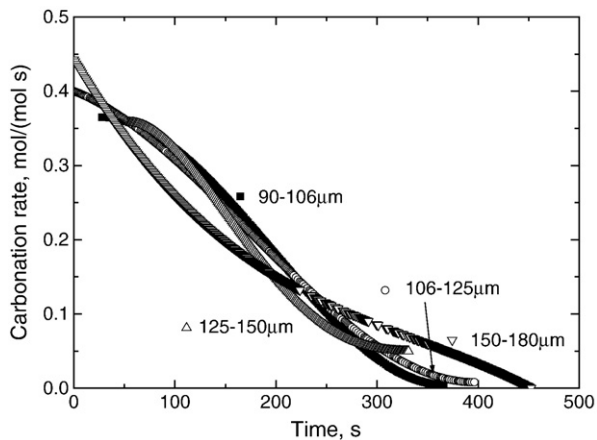


Fig. 8. Carbonation rates of particles of different size ranges. Maximum heating rate during calcination 10 °C/s; temperature 600 °C; superficial sweep gas velocity 0.51 and 0.60 m/s for calcination and carbonation, respectively.

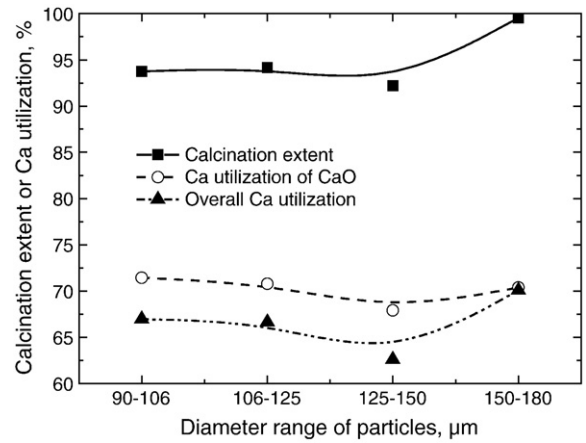


Fig. 9. Calcination extent and Ca utilization at different temperatures. Maximum heating rate during calcination 10 °C/s; final calcination temperature 850 °C; carbonation temperature 600 °C; superficial sweep gas velocity 0.51 and 0.60 m/s for calcination and carbonation, respectively.

trajectories, plotted in Fig. 15(a). Real-time sample weight and temperature were acquired during the calcination to analyze the effect of the initial heating rate on the calcination and subsequent carbonation for these two cases. Fig. 15(b) shows that calcination was significantly faster for case A, where the heating rate was nearly constant, than for case B, where the initial heating rate was considerably higher than the subsequent heating rate. The calcination extent then reached ~70% after very different time periods. These two samples were then exposed to carbonation, with the resulting overall Ca utilization vs. time results plotted in Fig. 16. The two samples are seen to have carbonated at similar rates, with the overall Ca utilization reaching ~48% during carbonation, corresponding to a Ca utilization of ~70%. Calcination was hindered during the initial heating at the higher heating rate, but had little subsequent effect on carbonation of the resulting CaO.

The different reaction rates during sulphation of resulting CaO are shown in Fig. 17. The temperature was held at 800 °C during the sulphation at concentrations of SO₂, N₂ and O₂ in the gas mixture of 2237 ppmv, 3.2% and 96.7%, respectively, with limestone that had been 30% calcined in the WMR. There were two high-heating-rate cases, as well as one at a much lower-heating rate. In one, the sample was heated once and then held for 70 s at the final temperature, whereas in the other, heating, maintaining the final temperature constant and cooling occurred three times, with the cumulative constant temperature–time again being 70 s.

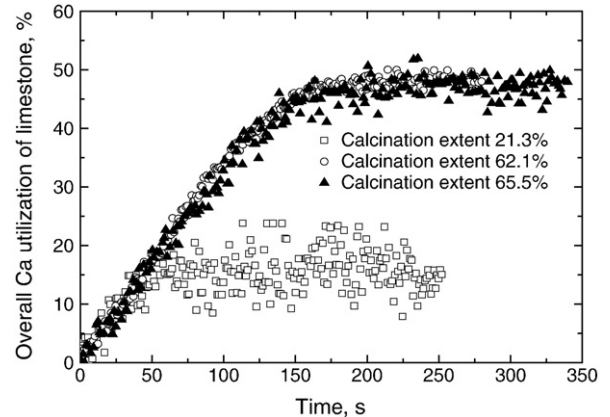


Fig. 10. Overall Ca utilization of limestone for carbonation after different extents of calcination of <63 μm limestone. Maximum heating rate during calcination 10 °C/s; carbonation temperature 600 °C; superficial sweep gas velocity 0.51 and 0.60 m/s for calcination and carbonation, respectively.

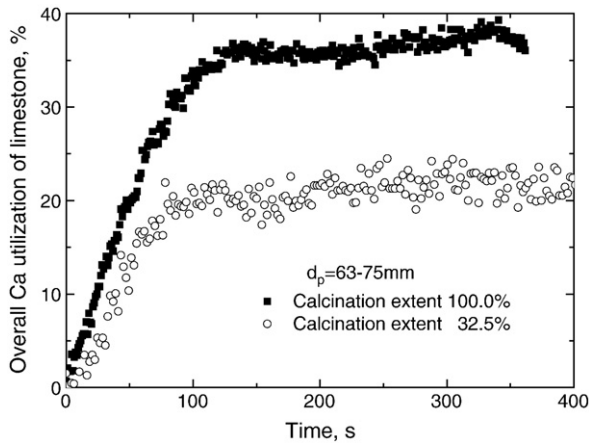


Fig. 11. Overall Ca utilization of limestone of diameter 63–75 μm for different calcination extents. Maximum heating rate 10 $^{\circ}\text{C}/\text{s}$; final calcination temperature 850 $^{\circ}\text{C}$; carbonation temperature 600 $^{\circ}\text{C}$; superficial sweep gas velocity 0.51 and 0.60 m/s for calcination and carbonation, respectively.

The sulphation rate for the rapidly resulting CaO was significantly lower than for the sorbent which had been calcined much more slowly. This suggests that the effect of rapid calcination is similar for carbonation and sulphation. Sulphation of limestone for the three-step discontinuous process was superior to that for a single continuous elevated temperature, as shown in Fig. 17. The reason may have been an increase of the surface area to volume ratio due to fragmentation of particles during the cyclic changes of temperature. Pores formed during the calcination of limestone may be plugged by the calcium sulphate in the outer product layer, further curbing sulphation, because the molar volume of CaSO_4 is greater than that of CaCO_3 . However, the outer gypsum product layer may crack during repeated heating and cooling, facilitating further sulphation.

The conversion of resulting CaO (shown in Fig. 18) was fitted to the equation

$$X = X_u[1 - a \exp\{-kt / X_u\}]. \quad (9)$$

The fitted constants are listed in Table 2 for limestone particles of diameter $<63 \mu\text{m}$ calcined at different heating rates. For both heating rates, the constant, a , is close to 1, the value obtained by both Gupta and Fan [35] and Bhatia and Perlmutter [34].

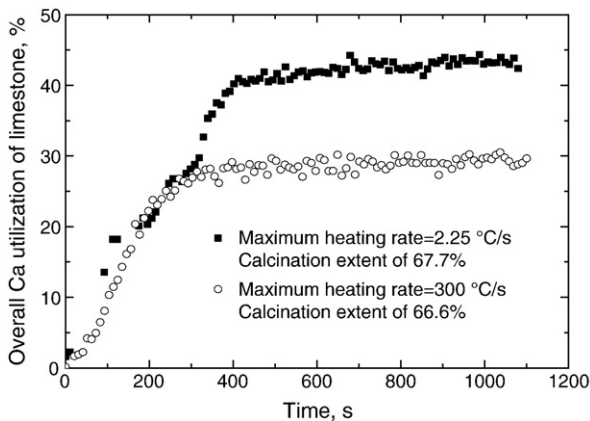


Fig. 12. Overall Ca utilization of $<63 \mu\text{m}$ limestone for carbonation after high and low heating rates during calcination; final calcination temperature 850 $^{\circ}\text{C}$; carbonation temperature 600 $^{\circ}\text{C}$; superficial sweep gas velocity 0.1, 0.51 and 0.60 m/s for rapid calcination, slow calcination and carbonation, respectively.

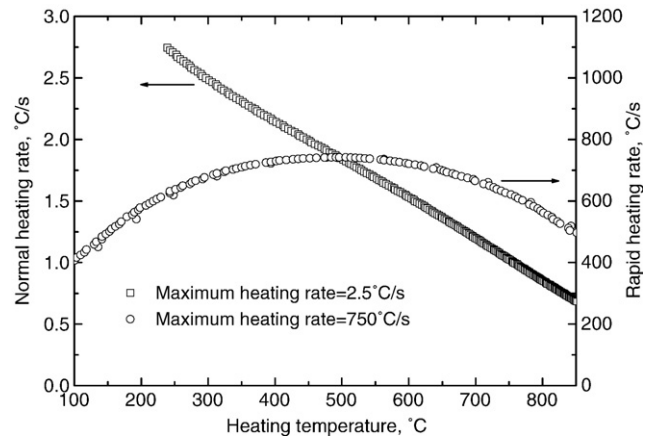


Fig. 13. Heating rate vs. temperature for two tests with 63–75 μm limestone. Final calcination temperature 850 $^{\circ}\text{C}$; carbonation temperature 600 $^{\circ}\text{C}$; superficial sweep gas velocity 0.1, 0.51 and 0.60 m/s for rapid calcination, slow calcination and carbonation, respectively.

7. Conclusions

Calcination of limestone heated in an electrically heated wire-mesh reactor and platinum foil reactor was studied to determine the effects of heating rate (0–800 $^{\circ}\text{C}/\text{s}$), calcination temperature (700–950 $^{\circ}\text{C}$), and particle size (0–180 μm) on the effectiveness of calcium-based sorbents for carbon capture via carbonation and sulphur capture via sulphation.

Of the temperatures studied, the best temperature to reach a high rate and favourable calcium utilization for carbonation was 607 $^{\circ}\text{C}$, after calcining limestone particles at a maximum heating rate of 10 $^{\circ}\text{C}/\text{s}$. Overall Ca utilization of the limestone reached its highest levels between 503 and 607 $^{\circ}\text{C}$. The rate of carbonation was faster at the beginning of the reaction and rapidly decreased from $\sim 0.6 \text{ mol}/(\text{mol s})$ to 0.04 $\text{mol}/(\text{mol s})$ within 300 s for carbonation temperatures of 503 to 607 $^{\circ}\text{C}$.

CaO produced by rapid calcination gave reduced rates of carbonation. Diffusion through the porous structure of the particles is likely to have been rate-limiting for both carbonation and sulphation. Overall Ca utilization of limestone and Ca utilization of CaO decreased significantly with increasing calcination heating rate. The sulphation rate was also lower for rapidly-calcined sorbent than

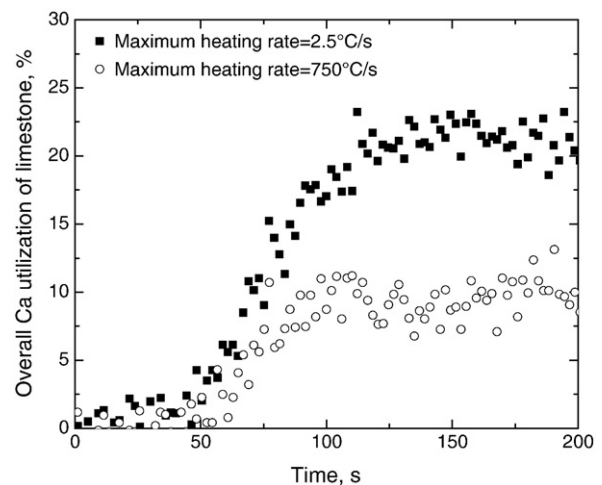


Fig. 14. Overall Ca utilization for two tests with 63–75 μm limestone. Final calcination temperature 850 $^{\circ}\text{C}$; carbonation temperature 600 $^{\circ}\text{C}$; superficial sweep gas velocity 0.1, 0.51 and 0.60 m/s for rapid calcination, slow calcination and carbonation, respectively. For heating rates vs. temperature see Fig. 13.

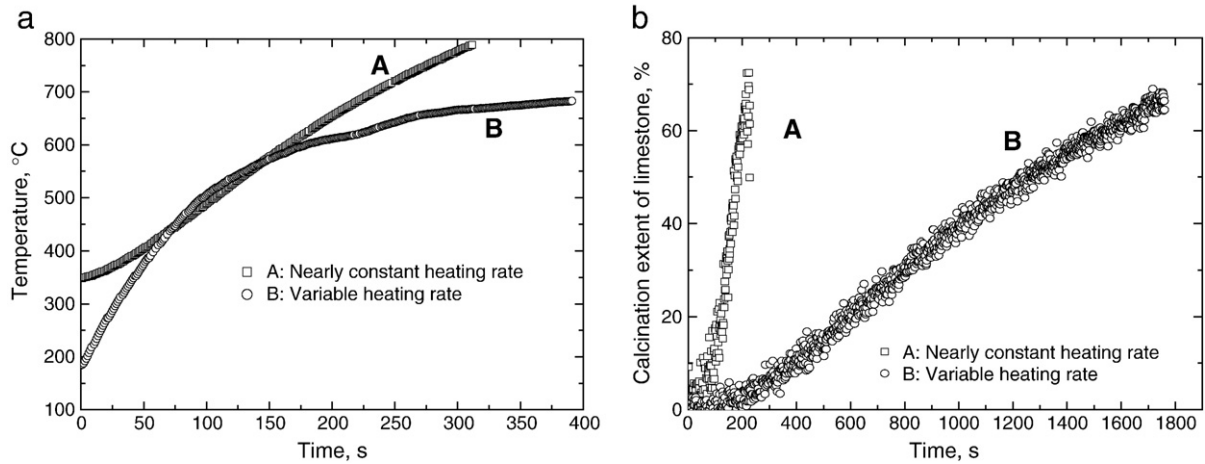


Fig. 15. Temperature and extent of calcination vs. time for <63 μm limestone for two very different cases. Final calcination temperature 850 °C; carbonation temperature 600 °C; superficial sweep gas velocity 0.51 and 0.60 m/s for calcination and carbonation, respectively.

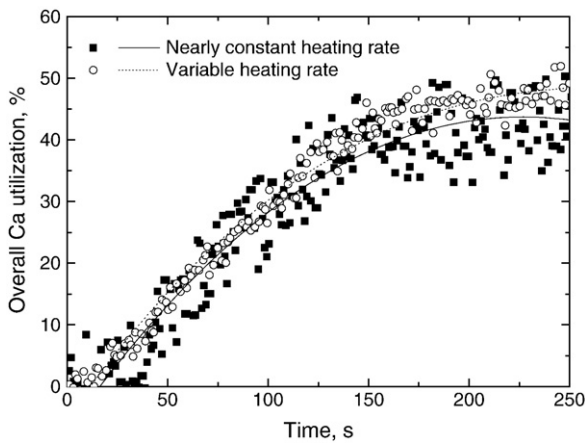


Fig. 16. Overall Ca utilization of <63 μm limestone after calcining at different heating rates as portrayed in Fig. 15. Final calcination temperature 850 °C; carbonation temperature 600 °C; superficial sweep gas velocity 0.51 and 0.60 m/s for calcination and carbonation, respectively.

for slowly-calcined sorbents, i.e. the effects of rapid calcination on carbonation and sulphation were similar. Calcination is hindered during initial heating at a higher heating rate, but there is little effect on the carbonation of the resulting CaO.

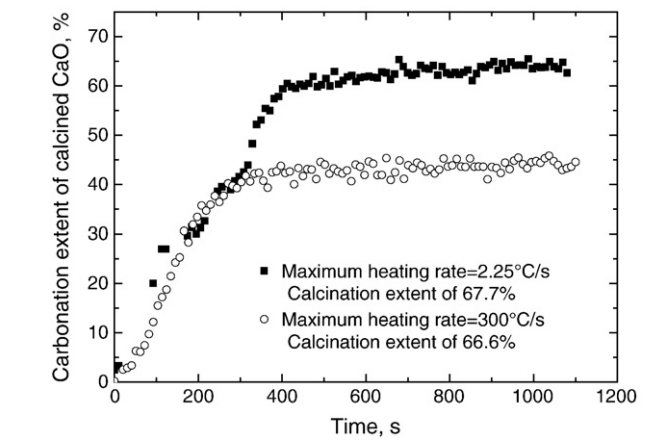


Fig. 18. Ca utilization of calcined CaO for <63 μm limestone particle on PFR for two different maximum heating rates; final calcination temperature 850 °C; carbonation temperature 600 °C; superficial sweep gas velocity 0.51 and 0.60 m/s for calcination and carbonation respectively.

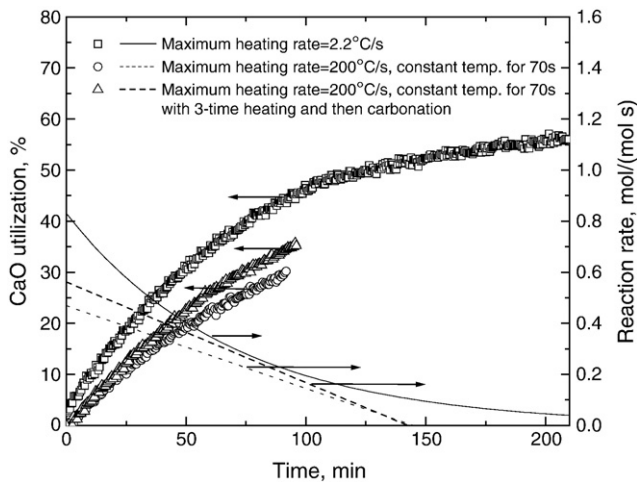


Fig. 17. Ca utilization of limestone for sulphation of limestone after three different calcination heating histories.

Nomenclature

- a* decay constant, dimensionless
- k* rate constant for CaO carbonation, mol m²/(s Pa)
- T* temperature, K
- t* time, s
- X_u* ultimate conversion of CaO, %

Acknowledgements

The authors are grateful to the National Natural Science Foundation of China (grant 50306026) and Guangzhou Science and Technology Bureau (grant 2006J1-C0421) for supporting C.F. Yan during this study, and to the Natural Sciences and Engineering Research Council of Canada for research funding.

Table 2
Reaction rate constant for carbonation.

Maximum heating rate (°C)	Maximum conversion, <i>X_u</i>	Constant, <i>a</i>	Reaction rate constant, <i>k</i> (s ⁻¹)
2.25	65.5	1.04	0.29
300	45.8	1.16	0.29

References

- [1] T.R. Ingraham, P. Marier, Kinetic studies on the thermal decomposition of calcium carbonate, *Can. J. Chem. Eng.* 41 (1963) 170–173.
- [2] A.B. Fuertes, G. Marban, F. Rubiera, Kinetics of thermal decomposition of limestone particles in a fluidized bed reactor, *Trans. Inst. Chem. Eng.* 71A (4) (1993) 421–428.
- [3] J.S. Dennis, A.N. Hayhurst, The effect of CO₂ on the kinetics and extent of calcination of limestone and dolomite particles in fluidized beds, *Chem. Eng. Sci.* 42 (10) (1987) 2361–2372.
- [4] G.D. Silcox, J.C. Kramlich, D.W. Pershing, A mathematical model for the Dash calcination of dispersed CaCO₃ and Ca(OH)₂ particles, *Ind. Eng. Chem. Res.* 28 (1989) 155–160.
- [5] R.H. Borgwardt, Calcination kinetics and surface area of dispersed limestone particles, *A.I.Ch.E. J.* 31 (1) (1985) 103–111.
- [6] J. Khinast, G.F. Krammer, C. Brunner, G. Staudinger, Decomposition of limestone: the influence of CO₂ and particle size on the reaction rate, *Chem. Eng. Sci.* 51 (4) (1996) 623–634.
- [7] T.R. Rao, D.J. Gunn, J.H. Bowen, Kinetics of calcium carbonate decomposition, *Chem. Eng. Res. Des.* 67 (1989) 38–47.
- [8] N. Hu, A.W. Scaroni, Calcination of pulverized limestone particles under furnace injection conditions, *Fuel* 75 (1996) 177–186.
- [9] K.M. Caldwell, P.K. Ghallager, D.W. Johnson, Effect of thermal transport mechanisms on the thermal decomposition of CaCO₃, *Thermochim. Acta* 18 (1977) 15–19.
- [10] M.C. Mai, T.F. Edgar, Surface area evolution of calcium hydroxide during calcination and sintering, *A.I.Ch.E. J.* 35 (1989) 30–36.
- [11] Y.H. Khraisha, D.R. Dugwell, Effect of water vapor on the calcination of limestone and raw meal in a suspension reactor, *Trans. Inst. Chem. Eng.* 69 (1991) 76–78.
- [12] J. Mu, D.D. Perlmutter, Thermal decomposition of carbonates, carboxylates, oxalates, acetates, formates, and hydroxides, *Thermochim. Acta* 49 (1981) 207.
- [13] A. Irabien, J.R. Viguri, F. Cortabitarte, I. Ortiz, Thermal dehydration of calcium hydroxide. 2. Surface area evolution, *Ind. Eng. Chem. Res.* 29 (1990) 1606–1611.
- [14] C.R. Milne, G.D. Silcox, D.W. Pershing, D.A. Kirchgessner, Calcination and sintering models for applications to high-temperature, short-time sulfation of calcium-based sorbents, *Ind. Eng. Chem. Res.* 29 (1990) 139–149.
- [15] E. Garcia-Calvo, M.A. Arranz, P. Leton, Effect of impurities in the kinetics of calcite decomposition, *Thermochim. Acta* 170 (1990) 7–11.
- [16] R.H. Borgwardt, K.R. Bruce, Effect of specific surface area on the reactivity of CaO with SO₂, *A.I.Ch.E. Ing. J.* 32 (2) (1986) 239–246.
- [17] D. Beruto, A.W. Searcy, Use of the Langmuir method for kinetic studies of decomposition reactions: calcite (CaCO₃), *Chem. Soc. J.* 70 (1974) 2145–2153 (Faraday Transaction).
- [18] A. Ghosh-Dastidar, S. Mahuli, R. Agnihotri, L.S. Fan, Ultrafast calcination and sintering of Ca(OH)₂ powder: experimental and modeling, *Chem. Eng. Sci.* 50 (1995) 2029–2040.
- [19] M. C. Mai, Analysis of simultaneous calcination, sintering, and sulfation of calcium hydroxide under furnace sorbent injection conditions. Ph.D. Thesis, Department of Chemical Engineering, University of Texas at Austin, Austin, TX, 1987.
- [20] V. Fierro, J. Adáñez, F. Garcáa-Labiano, Effect of pore geometry on the sintering of Ca-based sorbents during calcination at high temperatures, *Fuel* 83 (2004) 1733–1742.
- [21] Y.H. Khraisha, D.R. Dugwell, Thermal decomposition of Coudon limestone in a thermogravimetric analyser, *Chem. Eng. Res. Des.* 67 (1989) 48–51.
- [22] A.B. Fuertes, D. Alvarez, F. Rubiera, J.J. Pis, G. Marban, Simultaneous calcination and sintering model for limestone particles decomposition, *Trans. Inst. Chem. Eng.* 71A (1993) 69–76.
- [23] J.H. Wernick, Thermal dissociation pressure of calcium carbonate, *Min. Eng.* 6 (1954) 730–733.
- [24] K.B. Bischoff, Accuracy of the pseudo-steady-state approximation for moving boundary diffusion problems, *Chem. Eng. Sci.* 18 (1963) 711–715.
- [25] Irfan Ar, G. Dogu, Calcination kinetics of high purity limestones, *Chem. Eng. J.* 83 (2) (2001) 131–137.
- [26] C. Salvador, D. Lu, E.J. Anthony, J.C. Abanades, Enhancement of CaO for CO₂ capture in an FBC environment, *Chem. Eng. J.* 96 (1–3) (2003) 187–195.
- [27] J.C. Abanades, D. Alvarez, E.J. Anthony, D. Lu, In situ capture of CO₂ in a fluidized bed combustor, Proceedings of the 17th International (ASME) Conference on Fluidized Bed Combustion, Jacksonville, Florida, USA, May 18–21, 2003, pp. 133–135, Paper no. 10.
- [28] J. Wang, E.J. Anthony, J.C. Abanades, A simulation study for fluidised bed combustion of petroleum coke with CO₂ capture, Proceedings of the 17th International (ASME) Conference on Fluidized Bed Combustion, ASME, New York, 2003, (FBC2003-169).
- [29] T. Shimizu, T. Hiram, H. Hosoda, K. Kitano, M. Inagaki, K. Tejima, A twin fluid-bed reactor for removal of CO₂ from combustion processes, *Trans. Inst. Chem. Eng.* 77 (Part A) (1999) 62–68.
- [30] E.J. Anthony, Solid looping cycles: a new technology for coal conversion, *Ind. Eng. Chem. Res.* 47 (2008) 1747–1754.
- [31] P. Sun, J.R. Grace, C.J. Lim, E.J. Anthony, Removal of CO₂ by calcium-based sorbents in the presence of SO₂, *Energy Fuels* 21 (2007) 163–170.
- [32] D.K. Lee, An apparent kinetic model for the carbonation of calcium oxide by carbon dioxide, *Chem. Eng. J.* 100 (2004) 71–77.
- [33] P. Sun, J.R. Grace, C.J. Lim, E.J. Anthony, Determination of intrinsic rate constants of the CaO–CO₂ reaction, *Chem. Eng. Sci.* 63 (1) (2008) 47–56.
- [34] S.K. Bhatia, D.D. Perlmutter, Effect of the product layer on the kinetics of the CO₂–lime reaction, *A.I.Ch.E. J.* 29 (1983) 79.
- [35] H. Gupta, L.-S. Fan, Carbonation–calcination cycle using high reactivity calcium oxide for carbon dioxide separation from flue gas, *Ind. Eng. Chem. Res.* 41 (2002) 4035.
- [36] A.J. Dedman, A.J. Owen, Calcium cyanamide synthesis: Part 4. The reaction CaO + CO₂ = CaCO₃, *Trans. Faraday Soc.* 58 (1962) 2027–2035.
- [37] D. Mess, A.F. Sarofim, J.P. Longwell, Product layer diffusion during the reaction of calcium oxide with carbon dioxide, *Energy Fuels* 13 (1999) 999–1005.
- [38] S.-H. Wei, S.K. Mahuli, R. Agnihotri, L.-S. Fan, High surface area calcium carbonate: pore structural properties and sulfation characteristics, *Ind. Eng. Chem. Res.* 36 (1997) 2141–2148.
- [39] R. Barker, The reactivity of calcium oxide towards carbon dioxide and its use of energy storage, *J. Appl. Chem. Biotech.* 24 (1974) 221–227.
- [40] R. Loison, R. Chauvin, Pyrolyse Rapide du Charbon, *Chim. Ind.* 91 (1964) 269.
- [41] D.B. Anthony, J.B. Howard, H.P. Meissner, H.C. Hottel, Apparatus for determining high pressure coal-hydrogen reaction kinetics under rapid heating conditions, *Rev. Sci. Instrum.* 45 (1974) 992–995.
- [42] D.B. Anthony, J.B. Howard, H.C. Hottel, H.P. Meissner, Rapid devolatilization and hydrogasification of bituminous coal, *Fuel* 55 (1976) 121–128.
- [43] E.M. Suuberg, W.A. Peters, J.B. Howard, Product composition in rapid hydro-pyrolysis of coal, *Fuel* 59 (1980) 405–412.
- [44] W.S. Fong, W.A. Peters, J.B. Howard, Kinetics of generation and destruction of pyridine extractables in a rapidly pyrolyzing bituminous coal, *Fuel* 65 (1986) 251–254.
- [45] J.R. Gibbins, R. Kandiyoti, The effect of variations in time-temperature history on product distribution from coal pyrolysis, *Fuel* 68 (1989) 895–903.
- [46] J.R. Gibbins, R.A.V. King, R.J. Wood, R. Kandiyoti, Variable-heating-rate wire-mesh pyrolysis apparatus, *Rev. Sci. Instrum.* 60 (1989) 1129–1139.
- [47] J. Gibbins-Matham, R. Kandiyoti, Coal pyrolysis yields from fast and slow heating in a wire-mesh apparatus with a gas sweep, *Energy Fuels* 2 (1988) 505–511.
- [48] C.J. Hindmarsh, K.M. Thomas, W.X. Wang, H.Y. Cai, A.J. Guell, D.R. Dugwell, R. Kandiyoti, A comparison of the pyrolysis of coal in wire-mesh and entrained-flow reactors, *Fuel* 74 (1995) 1185–1190.
- [49] J.Y. Lim, I.N. Chatzakis, A. Megaritis, H.Y. Cai, D.R. Dugwell, R. Kandiyoti, Gasification and char combustion reactivities of Daw Mill coal in wire-mesh and hot-rod reactors, *Fuel* 76 (1997) 1327–1335.
- [50] C. Mill, Pyrolysis of fine coal particles at high heating rate and pressure, PhD thesis, University of New South Wales, Australia, Sept. 2000.
- [51] P.R. Solomon, M.A. Serio, E.M. Suuberg, Coal pyrolysis: experiments, kinetic rates and mechanisms, *Prog. Energy Combust. Sci.* 18 (1992) 133–220.
- [52] K. Laursen, W. Duo, J.R. Grace, C.J. Lim, Sulfation and reactivation characteristics of nine limestones, *Fuel* 79 (2000) 153–163.
- [53] N. Hu, A.W. Scaroni, Fragmentation of calcium-based sorbents under high heating rate, short residence time conditions, *Fuel* 74 (1995) 374–382.
- [54] P. Sun, J.R. Grace, C.J. Lim, E.J. Anthony, A discrete-pore-size-distribution-based gas–solid model and its application to the CaO + CO₂ reaction, *Chem. Eng. Sci.* 63 (1) (2008) 57–70.
- [55] P. Sun, C.J. Lim, J.R. Grace, Cyclic CO₂ capture by limestone-derived sorbent during prolonged calcination/carbonation cycling, *A.I.Ch.E. J.* 54 (2008) 1668–1677.
- [56] S.J. Bortz, P. Flament, Recent IFRF fundamental and pilot-scale studies on the direct sorbent injection process, Proceedings: First Joint Symposium on Dry SO₂ and Simultaneous SO₂–NO_x Control Technologies, 1985, pp. 17–1–17–22, Vol. 1, EPA-600/9-85/020a.